Progress In Electromagnetics Research C, Vol. 112, 127–137, 2021

Wide-Band Log-Periodic Microstrip Antenna with Defected Ground Structure for C-Band Applications

Kunal K. Upadhyay, Alkesh Agrawal*, and Mukul Misra

Abstract—The manuscript presents a log-periodic microstrip antenna with a defective ground structure (LPMADGS). The antenna is simulated, designed, and validated for C-band applications. The design of the antenna consists of three layers with upper most layer consisting of log-periodic, copper patches with a thickness of 0.035 mm; the middle layer is a 2 mm thick dielectric layer of FR-4 substrate; and the bottom layer is a defected ground structure (concentric ring resonators of 0.035 mm thickness). The suggested antenna design is simulated with a complete ground plane, without ground plane, and with a defective ground plane. The proposed antenna with optimized design is fabricated by wet etched method. The simulated results are approximately similar to the experimentally measured results. The experimentally measured results show transmission peaks at 7.65 GHz and 7.90 GHz. The resonating effect of log-periodic patches with a defected ground structure results in wide-band of 0.91 GHz (−10 dB bandwidth). The proposed antenna structure exhibits a wide bandwidth transmission which mostly resonates in frequency range that lies in C-band. It has future applications for mobile as well as wireless communication.

1. INTRODUCTION

Research in the area of microstrip antennas is advancing due to their thin planar profile, ease of surface mounting on missiles and aircrafts [1, 2], ease of fabrication process [3–5], and ease of integrating the antenna on the same printed board with other components, especially in mobile radio communication devices [6–8]. The most common type of microstrip antenna is three-layered patch antenna with square [9], circular [10], rectangular [11, 12], elliptical [7, 8], or any other shaped patch [13] with matched feed line on the top, middle dielectric layer separating the bottom ground plane from the top layer. The antennas with microstrip patches can find applications in GPS [10, 14, 15], mobile devices [7, 8, 11–13, 17], WLAN [5, 11, 13–16], and WiMax [5, 13, 15, 16]. The patch antennas are found to have low gain and narrow bandwidth [12–15]. The concept of log-periodic structure is often utilized to achieve the broad-band performance of antenna in microwave and THz frequency range [18–22]. The dimensions of the bottom ground plane affect the antenna bandwidth [23]. The benefit of a defected ground structure (DGS) is reduced antenna size and improvement in the patch antenna bandwidth [24]. Keeping in mind these facts, a new design (LPMADGS) is proposed with log-periodic patches on the top and CCRRs (DGS) at the bottom layer. The new proposed design results in broad-band resonance transmission peaks and appreciable high gain.

Received 11 March 2021, Accepted 28 April 2021, Scheduled 2 May 2021
* Corresponding author: Alkesh Agrawal (alkesh.agrawal26@gmail.com).
The authors are with the Faculty of Electronics and Communication Engineering, Institute of Technology, Shri Ramswaroop Memorial University, Barabanki, India.

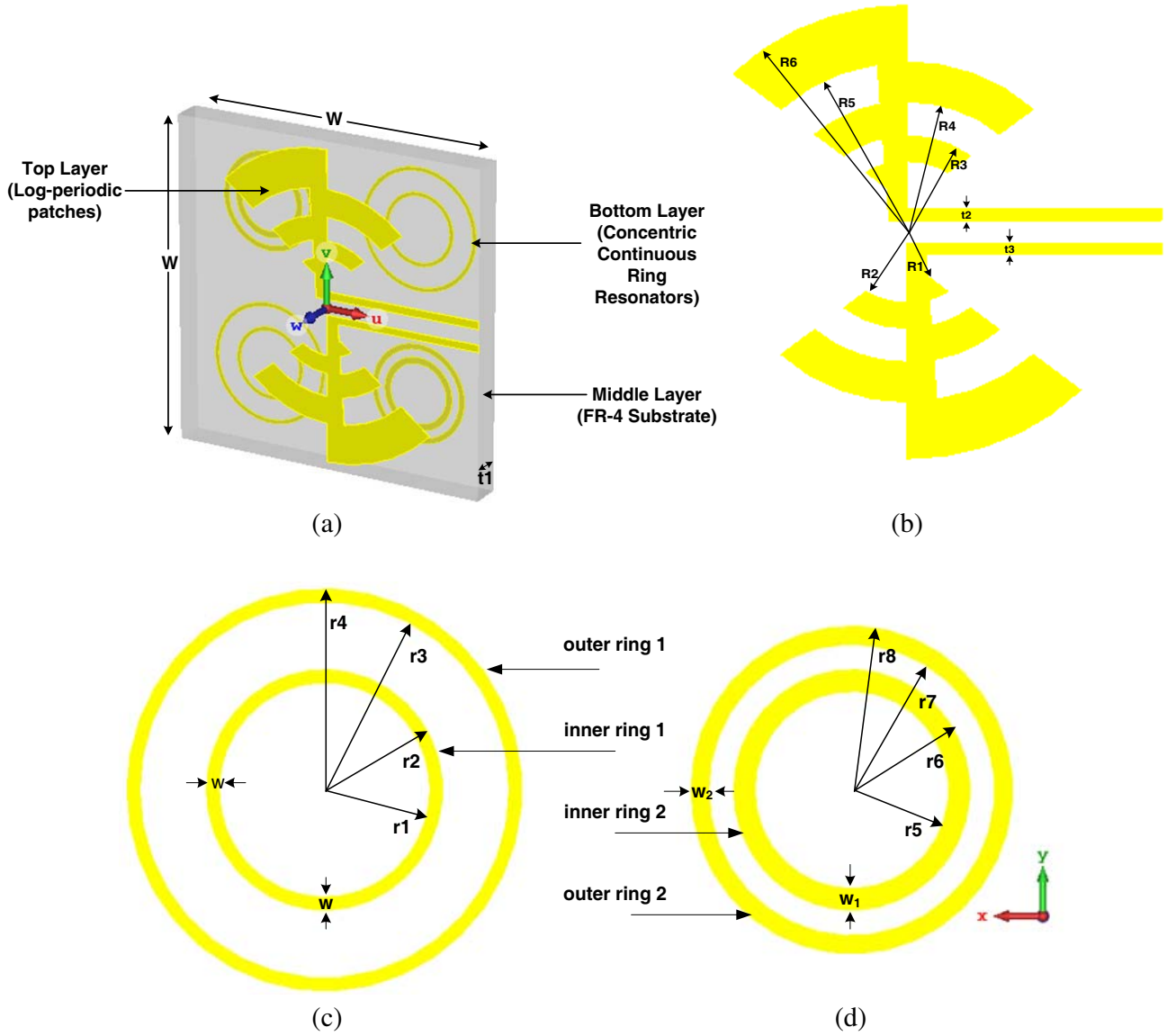

Figure 1. (a) Three dimensional design of LPMADGS. (b) Dimensions of top layered log-periodic patches. (c) Outer and inner ring 1 dimension [25]. (d) Outer and inner ring 2 dimension [25].

2. THE STRUCTURE, EQUIVALENT MODEL AND SIMULATION OF LPMADGS

The proposed configuration of the CCRR-loaded log-periodic patch antenna is a three-layered structure as can be seen in Figure 1(a). The top layer consists of log-periodic patches with different radii which form the antenna structure and can be seen in Figure 1(b). The lower layer consists of four pairs of continuous copper ring resonators with different radii [25], positioned in all four quadrants shown in Figures 1(c) and 1(d) which form the DGS. The middle layer consists of an FR-4 substrate (relative permittivity 4.4, loss tangent 0.02, and thickness 2 mm). CST microwave studio software is used to simulate the optimized design, breaking the structure into 38,812 tetrahedron meshes.

The parameters R_1, R_2, R_3, R_4, R_5, and R_6 are the radii of the log-periodic patches increasing in value from R_1 to R_6 with $(R_{n+i}/R_n) = 1.3$, and t_2 and t_3 are thickness of teeth strips of log-periodic structure which act as feedlines. The optimized dimensions of the proposed structure are depicted in Table 1. For CCRRs, the optimized dimensions are depicted in Table 2, and w ($r_2 - r_1$ and $r_4 - r_3$),

Table 1. Optimize dimensions of LPMADGS.

Parameter	Dimension (mm)
W	21
R_6	10
R_5	7.5
R_4	5.75
R_3	4.25
R_2	3.125
R_1	2.25
t_1	2.00
t_2	0.50
t_3	0.45

Table 2. Optimize dimensions of DGS [25].

Parameter	Dimension (mm)	Parameter	Dimension (mm)
r_1	2.10	r_7	2.85
r_2	2.35	r_8	3.20
r_3	3.68	w	0.25
r_4	3.93	w_1	0.42
r_5	1.93	w_2	0.35
r_6	2.35		

w_1 $(r_6 - r_5)$, and w_2 $(r_8 - r_7)$ are the thicknesses of the respective inner ring 1, outer ring 1, inner ring 2, and outer ring 2.

The design process is based on the design calculation approximations given in [26]. The approximate element lengths of the LPMADGS are calculated using Equations (1)–(6), where ε_{eff} and ε_r are the effective and relative permittivities of the substrate; h is the width of the substrate; w_s is the width of the feed strip line; $L_{\max}$ is the maximum length of the element; K_1 is the upper truncation constant [26]; f_{upper} is upper frequency spectral component; f_{lower} is the lower frequency spectral component (that defines the bandwidth $= f_{\text{upper}} - f_{\text{lower}}$); $\lambda_{\max}$ is the maximum wavelength value corresponding to f_{lower}.

$$\varepsilon_{eff} = \frac{\varepsilon_r + 1}{2} + \frac{\varepsilon_r - 1}{2} * \frac{1}{\sqrt{1 + \frac{10h}{W_s}}} \tag{1}$$

$$L_{\max} = K_1 \lambda_{\max} \tag{2}$$

$$\lambda_{\max} = \frac{c}{\sqrt{\varepsilon_{eff}} * f_{\text{lower}}} \tag{3}$$

$$K_1 = 1.01 - 0.519\tau \tag{4}$$

$$\tau = \frac{f_{\text{lower}}}{f_{\text{upper}}} \tag{5}$$

$$L_n = \tau * L_{n+1} \tag{6}$$

Figure 2 shows the equivalent circuit model of top layered patch of the proposed LPMADGS. The feed strip line is modeled as a transmission line equivalent with inductor in series and capacitor in parallel, in order to have a lossy structure there is parallel connection of resistor and capacitor as shown in Figure 2. The individual element of the microstrip patch antenna is modeled as (r, l, c) parallel

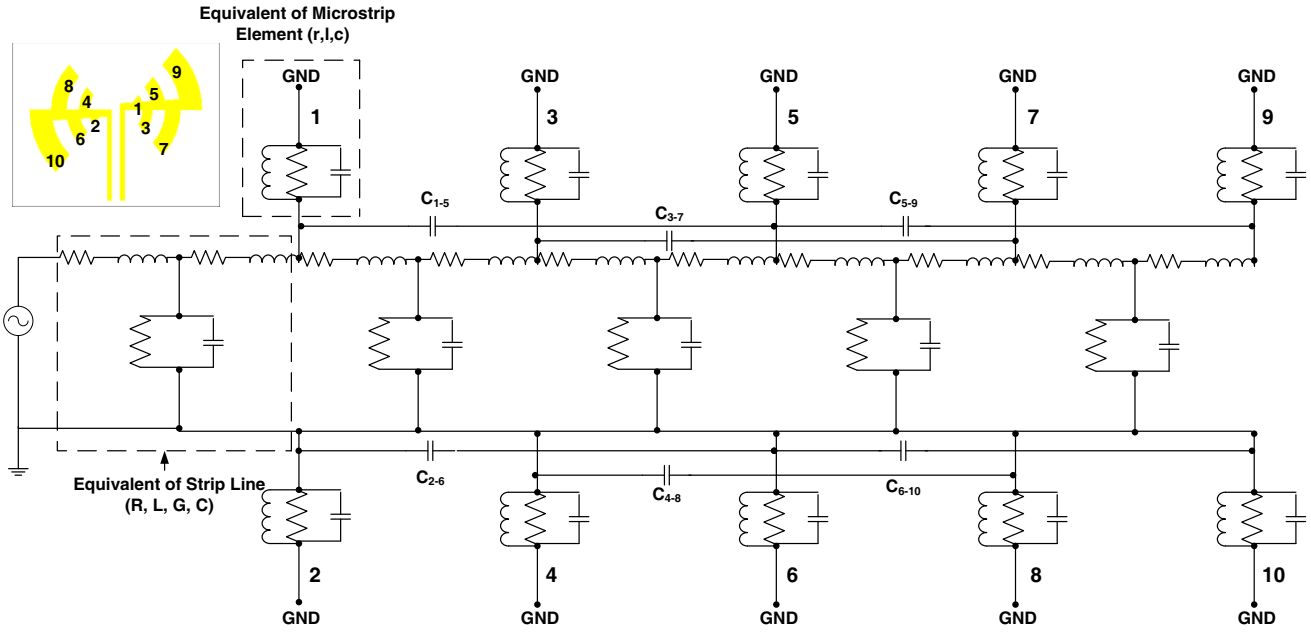

Figure 2. Equivalent circuit model of top layered patch of LPMADGS.

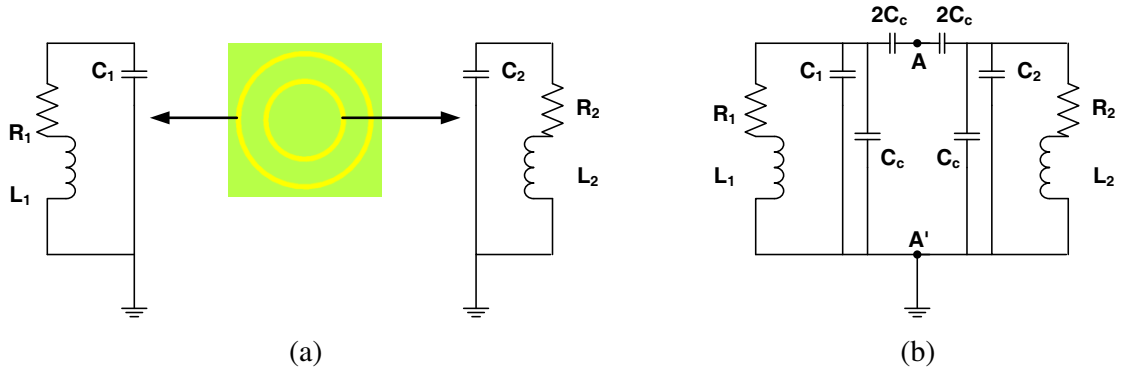

Figure 3. (a) Equivalent circuit model of individual ring resonator. (b) Equivalent circuit model of bottom layered structure of LPMADGS.

resonant circuit [27, 28]. Since there is EM coupling between individual elements on the same side of the feed strip line, they are connected through coupling capacitors ($C_{1–5}$, $C_{3–7}$, $C_{5–9}$, $C_{2–6}$, $C_{4–8}$, $C_{6–10}$) as shown in Figure 2. The equivalent circuit model of each ring resonator is shown in Figure 3(a). The two ring resonators are coupled together by coupling capacitor (C_c), and the equivalent circuit model is shown in Figure 3(b).

Open boundary conditions are applied along the x-direction, y-direction, and z-direction as shown in Figure 4. The proposed patch antenna was simulated in three different configurations with a complete ground plane, without ground plane, and with a defected ground plane at the bottom layer. From the results shown in Figure 5, it is clear that proposed patch antenna without ground plane resonates at 8.49 GHz, with complete ground plane resonates at 5.82 GHz and 8.91 GHz, and with defected ground plane, the patch antenna resonates at 7.575 GHz and 8.64 GHz with return loss values of −15.41 dB and −15.04 dB, respectively. Within the frequency range from 5 to 12 GHz, the CCRRs exhibited reflection coefficients at 7.35 GHz and 8.91 GHz. The proposed LPMADGS structure resulted in merged resonance peaks (CCRRs and top layered log-periodic patch) to give broad bandwidth of 1.5 GHz (−10 dB).

In order to study the resonance mechanism, the surface current distributions of the LPMADGS structure at resonance frequencies of 7.575 GHz and 8.64 GHz are studied as shown in Figure 6. When

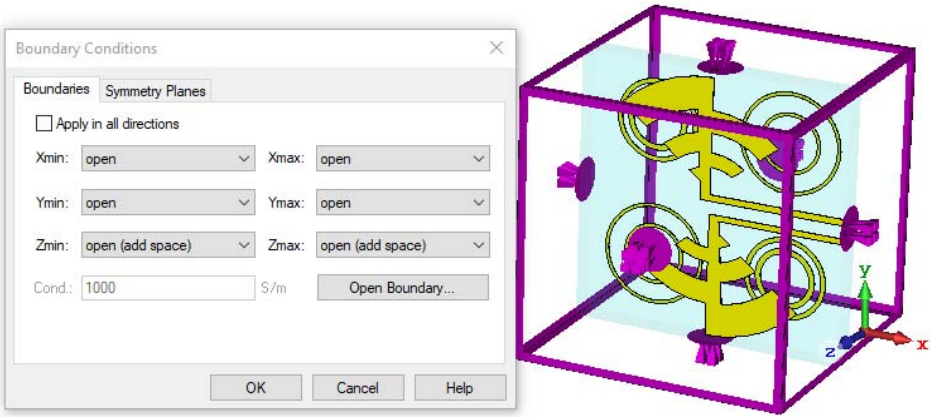

Figure 4. Applied boundary conditions in x, y and z directions.

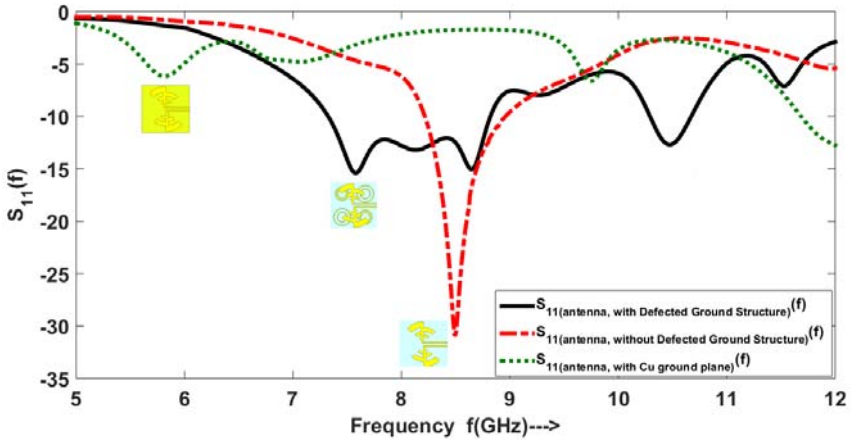

Figure 5. Simulated reflection coefficients.

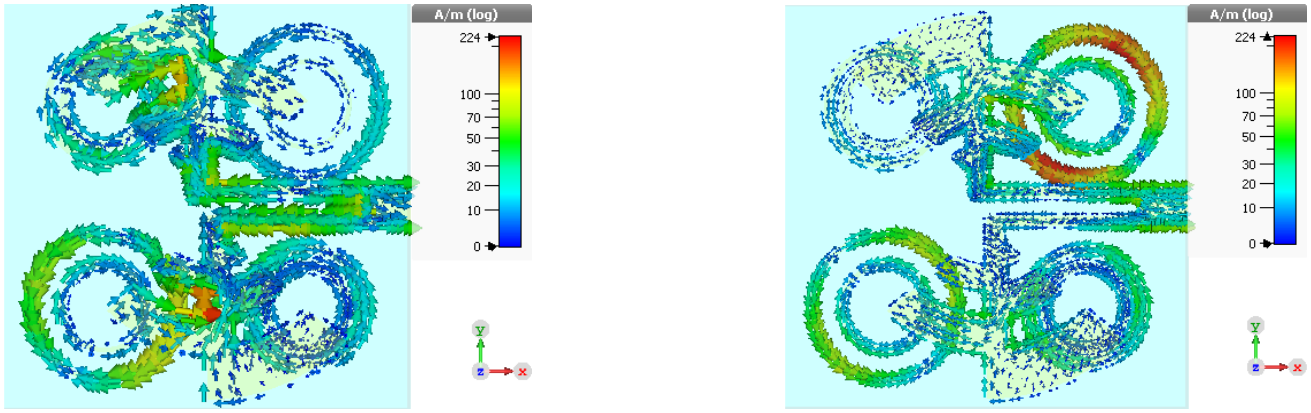

(a) (b)

Figure 6. Surface current distribution of the proposed antenna at (a) 7.575 GHz, (b) 8.64 GHz.

the suitable power is fed at one port of LPMADGS, surface currents are generated on the log-periodic patches as well as on the concentric continuous ring resonators as shown in Figure 6. The arrow indicates flows of surface current within log periodic patches at the top surface and concentric continuous

ring resonators at the bottom. The induced surface current distributions further induces electric and magnetic fields [29], and following the maximum power transfer theorem the confined surface currents within the antenna structure get converted into EM waves, hence the proposed LPMADGS radiates maximum at 7.575 GHz and 8.64 GHz. It is observed from Figure 4 that the transverse magnetic mode radiation was generated by log-periodic patches combined with the transverse magnetic mode radiation generated by the CCRRs [30] and resulted in wide-band property (depicted in Figure 5).

Figures 7(a) and 7(b) show 2D polar plots of the LPMADGS at resonance frequencies 7.575 GHz and 8.64 GHz. The LPMADGS is oriented in xy-plane. The strength of electric field is in z-direction when antenna is in co-plane (phi = 0), and when antenna is in cross-plane (phi = 90) the polarization of electric field gets orthogonal with respect to co-plane. In both co- and cross-polarizations, the orientation of electric field gets reversed.

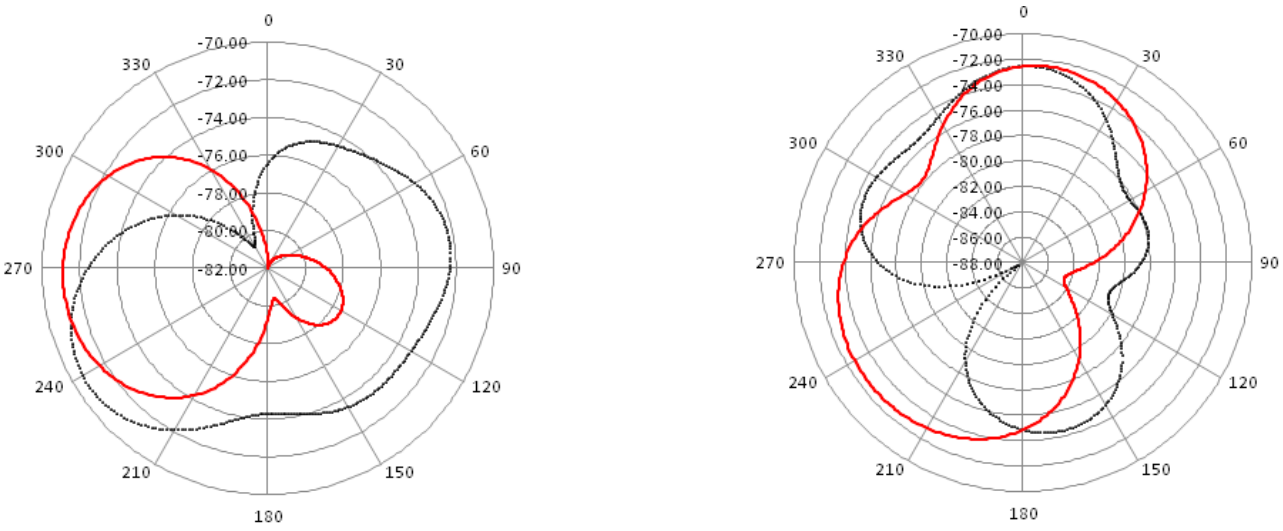

Figure 7. 2D polar plot at all the resonance frequencies (a) at 7.575 GHz, (b) at 8.64 GHz.

3. EXPERIMENT

The LPMADGS structure is fabricated on a double sided copper laminated FR-4 substrate (relative permittivity 4.4, loss tangent 0.02, and thickness 2 mm) by photo-lithographic method followed by wet etching process [25] with dimensions 21 mm × 21 mm × 2 mm shown in Figure 8.

The fabricated LPMADGS structure is experimentally tested in an anechoic chamber with the help of Vector Network Analyzer (VNA) and Horn antenna. Port 1 of VNA is connected to the SMA connector of LPMADGS for calculating input reflection coefficient as shown in Figure 9(a) and Figure 9(b). The fabricated antenna is placed inside an anechoic chamber for far field calculations. The LPMADGS is placed in front of the horn antenna which is placed on a rotating disc machine as shown in Figure 9(c) and Figure 9(d). The rotating disc machine connected to VNA was placed in microwave lab. LPMADGS acted as the transmitting antenna in the space inside the anechoic environment, and the horn antenna acted as the receiving antenna. Both antennas are placed at a distance of approximately one meter as shown in Figure 9(d).

To eliminate the impact of near-far field and the diffraction effects on the measurements, the position of LPMADGS under test (in front of the receiving antenna) is decided. In order to measure the radiation patterns, co-planar and cross-planar polarized orientations of E-field and H-field are generated by rotating the LPMADGS and the horn antenna placed front to front by feeding the instructions by the computer. In co-planar position, both LPMADGS and horn antenna are aligned in same direction with respect to E-field and H-field orientations, and in cross-planar position both the antennas are orthogonal to each other with respect to E-field and H-field orientations.

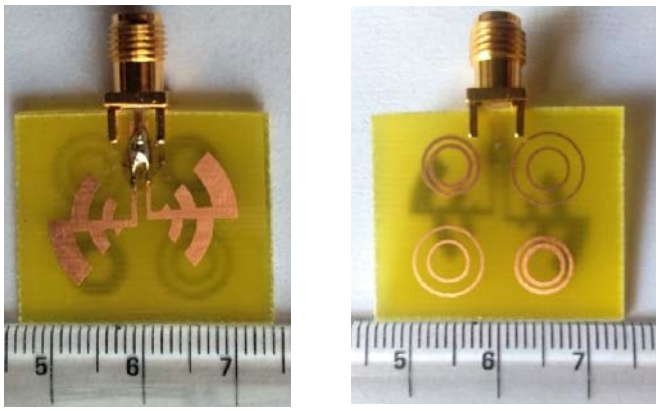

(a) (b)

Figure 8. The fabricated LPMADGS structure with (a) top view, (b) bottom view.

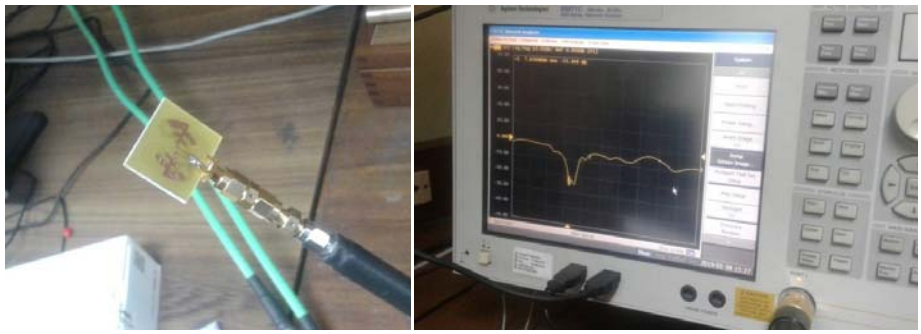

(a) (b)

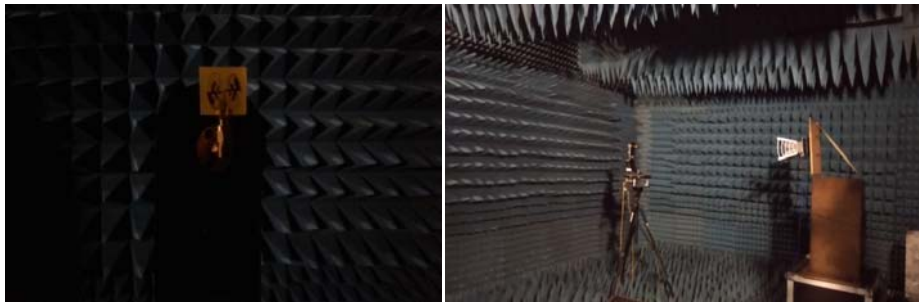

(c) (d)

Figure 9. The testing arrangement. (a) Applied voltage at port 1 to calculate return loss. (b) Return loss measurement by VNA (Agilent technologies E5071C, 300 kHz–20 GHz). (c) LPMADGS fixed on rotating disc. (d) Fixed LPMADGS on rotating disc in front of the horn antenna.

4. RESULTS

The resonance frequencies of proposed LPMADGS are measured experimentally [shown in Figure 10(a)] and compared with the simulated results shown in Figure 10(b) which meets the −10 dB requirement. There is a small deviation between simulated and measured results, i.e., measured resonance frequencies are 7.65 GHz and 7.90 GHz, while simulated resonance frequencies are 7.575 GHz and 8.64 GHz due to manufacturing errors. Figures 11(a), 11(b), and 11(c) show comparison of simulated and experimentally measured radiation patterns in terms of 2D polar plots of LPMADGS at resonance frequencies 7.65 GHz,

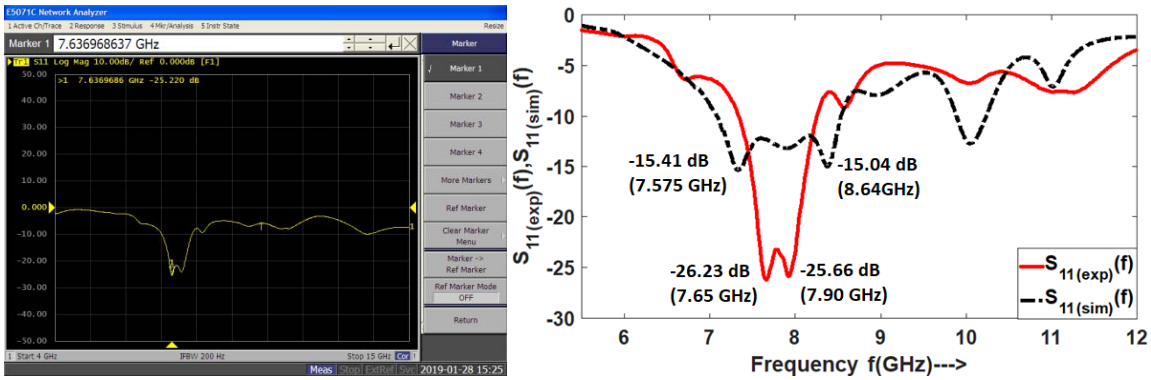

Figure 10. (a) Measured reflection coefficient in VNA (Agilent Technologies E5071C, 300 kHz–20 GHz). (b) Simulated and measured reflection coefficient (S_{11}) of the proposed LPMADGS.

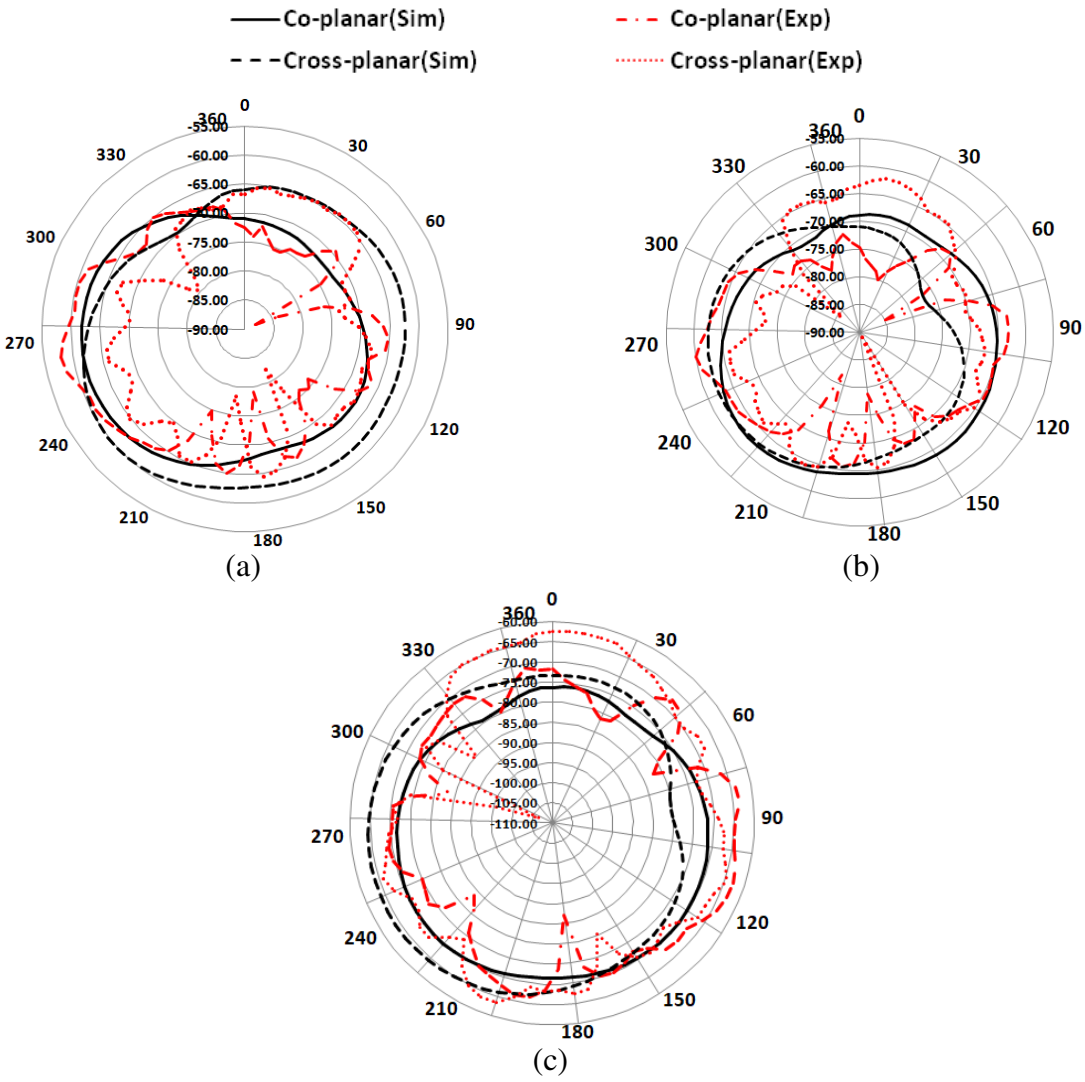

Figure 11. Experimentally measured and simulated co-planar and cross-planar radiation patterns at resonance frequencies (a) 7.65 GHz, (b) 7.76 GHz, (c) 7.90 GHz.

Table 3. Comparison of simulated and measured input reflection coefficients of the LPMADGS.

Simulated Results		**Obtained Results**	
Resonance Frequency (GHz)	**S_{11} (dB)**	**Resonance Frequency (GHz)**	**S_{11} (dB)**
7.575	−15.41	**7.65**	−26.23
8.64	−15.04	**7.90**	−25.66
Simulated Bandwidth: 1.50 GHz		**Measured Bandwidth:** 0.91 GHz	

7.76 GHz, and 7.90 GHz. The LPMADGS is in xy-plane whereas the strength of electric field is oriented along z-direction in co-plane (phi = 0), and when antenna is in cross-plane (phi = 90) the polarization of electric field gets oriented orthogonally with respect to co-plane. The radiation pattern shows the omnidirectional characteristics shown in Figure 11 (for both simulated and experimentally measured results) which were considered as appropriate for wireless technologies in the C-band.

5. CONCLUSION

A new design of log-periodic patch antenna with defected ground plane exhibiting wide-band characteristic is simulated in CST microwave studio, fabricated on a double sided FR-4 substrate, and experimentally tested in an anechoic chamber using a horn antenna and vector network analyzer. The proposed patch antenna was simulated with ground plane, without ground plane, and with DGS at the bottom layer. The patch antenna with DGS at the bottom layer resonated at 7.65 GHz and 7.90 GHz. Table 3 shows the simulated values of reflection coefficients at corresponding resonance frequencies: −15.41 dB ($f_1 = 7.575$ GHz) and −15.04 dB ($f_2 = 8.64$ GHz), whereas the experimental values of input reflection coefficients at their corresponding resonance frequencies are −26.23 dB ($f_1 = 7.65$ GHz) and −25.66 dB ($f_2 = 7.90$ GHz) suitable for C-band applications. The proposed antenna showed wide-band reflection coefficients (0.91 GHz) in C-band with omnidirectional radiation patterns in co- and cross-polarization states.

ACKNOWLEDGMENT

The authors are very grateful to Prof. (Dr.) K. V. Srivastava for providing adequate resources for the smooth conduction of current research work in the Microwave Lab at IIT Kanpur, Department of Electrical Engineering.

REFERENCES

1. Gupta, S. D. and M. C. Srivastava, "Design of frequency agile multidielectric microstrip antenna for airborne applications," *International Journal of Microwave and Optical Technology (IJMOT)*, Vol. 5, 257–266, 2010.
2. Wu, J., J. Yu, and Q. Tao, "Design of a missile-borne conformal microstrip navigation antenna," *MATEC Web of Conferences*, Vol. 232, 04080, 2018.
3. Jan, J. Y. and J. W. Su, "Bandwidth enhancement of a printed wide-slot antenna with a rotated slot," *IEEE Transactions on Antennas and Propagation*, Vol. 53, 2111–2114, 2005.
4. Liu, Y. F., K. L. Lau, Q. Xue, and C. H. Chen, "Experimental studies of printed wide-slot antenna for wide-band applications," *IEEE Antennas Wireless Propagation Letters*, Vol. 3, 273–275, 2004.
5. Chen, W. S. and K. Y. Ku, "Band-rejected design of printed open slot antenna for WLAN/WiMAX operation," *IEEE Transactions on Antennas and Propagation*, Vol. 56, No. 4, 1163–1169, 2008.
6. Chattha, H. T., M. Hanif, X. Yang, Q. H. Abbasi, and I. E. Rana, "Frequency reconfigurable patch antenna for 4G LTE applications," *Progress In Electromagnetics Research M*, Vol. 69, 1–13, 2018.

7. Khattak, M. I., A. Sohail, U. Khan, Z. Ullah, and G. Witjaksono, "Elliptical slot circular patch antenna array with dual band behaviour for future 5G mobile communication networks," *Progress In Electromagnetics Research C*, Vol. 89, 133–147, 2019.
8. Alieldin, A., Y. Huang, S. J. Boyes, and M. Stanley, "A reconfigurable broadband dual-mode dual-polarized antenna for sectorial/omnidirectional mobile base stations," *Progress In Electromagnetics Research*, Vol. 163, 1–13, 2018.
9. Alqadami, A. S. M., M. F. Jamlos, I. Islam, P. J. Soh, R. Mamat, K. A. Khairi, and A. Narbudowicz, "Multi-band antenna array based on double negative metamaterial for multi automotive applications," *Progress In Electromagnetics Research*, Vol. 159, 27–37, 2017.
10. Naik, K. K. and P. A. Vijaya Sri, "Design of hexadecagon circular patch antenna with DGS at Ku band for satellite communications," *Progress In Electromagnetics Research M*, Vol. 63, 163–173, 2018.
11. Selvi, N. T., R. Pandeeswari, and P. N. T. Selvan, "An inset-fed rectangular microstrip patch antenna with multiple split ring resonator loading for WLAN and RF-ID applications," *Progress In Electromagnetics Research C*, Vol. 81, 41–52, 2018.
12. Saroj, A. K., M. G. Siddiqui, M. Kumar, and J. Ansari, "Design of multiband quad-rectangular shaped microstrip antenna for wireless applications," *Progress In Electromagnetics Research M*, Vol. 59, 213–221, 2017.
13. Jabar, A. A. S. A. and D. K. Naji, "Design of miniaturized quad-band dual-arm spiral patch antenna for RFID, WLAN and WiMAX applications," *Progress In Electromagnetics Research C*, Vol. 91, 97–113, 2019.
14. Khajepour, S., M. S. Ghaffarian, and G. Moradi, "Design of novel multiband folded printed quadrifilar helical antenna for GPS/WLAN applications," *IEEE Electronics Letters*, Vol. 53, No. 2, 58–60, 2017.
15. Sun, X., G. Zeng, H.-C. Yang, Y. Li, X.-J. Liao, and L. Wang, "Design of an edge-fed quad-band slot antenna for GPS/WiMAX/WLAN applications," *Progress In Electromagnetics Research Letters*, Vol. 28, 111–120, 2012.
16. Yu, J., Y. Sun, H. Zhu, F. Li, and Y. Fang, "Stacked-patch dual-band & dual-polarized antenna with broadband baluns for WiMAX & WLAN applications," *Progress In Electromagnetics Research M*, Vol. 68, 41–52, 2018.
17. Liu, C. S., C. N. Chiu, and S. M. Deng, "A compact disc-slit monopole antenna for mobile devices," *IEEE Antennas and Wireless Propagation Letters*, Vol. 7, 251–254, 2008.
18. Kumar, H. and G. Kumar, "A broadband planar modified quasi-Yagi using log-periodic antenna," *Progress In Electromagnetics Research Letters*, Vol. 73, 23–30, 2018.
19. Dykaar, D. R., B. I. Greene, J. F. Federici, A. F. J. Levi, L. N. Pfeiffer, and R. F. Kopf, "Log-periodic antennas for pulsed terahertz radiation," *Appl. Phys. Lett.*, Vol. 59, 262, 1991.
20. Haraz, O. M., "Millimeter-wave printed dipole array antenna loaded with a low-cost dielectric lens for high-gain applications," *Journal of Infrared, Millimeter, and Terahertz Waves*, Vol. 41, No. 3, 225–244, 2020.
21. Haraz, O. M., A. R. Sebak, and S. Alshebeili, "Study the effect of using low-cost dielectric lenses with printed log-periodic dipole antennas for millimeter-wave applications," *International Journal of Antennas and Propagation*, Vol. 2015, 1–7, 2015.
22. Haraz, O. M., S. A. Alshebeili, and A.-R. Sebak, "Low-cost high gain printed log-periodic dipole array antenna with dielectric lenses for V-band applications," *IET Microwaves, Antennas & Propagation*, Vol. 9, No. 6, 541–552, 2015.
23. Hasan, M. M., M. R. I. Faruque, and M. T. Islam, "Dual band metamaterial antenna for LTE/Bluetooth/WiMAX system," *Scientific Reports (Nature)*, Vol. 8, No. 1240, 1–17, 2018.
24. Kushwaha, N. and R. Kumar, "An UWB fractal antenna with defected ground structure and Swastika shape electromagnetic band gap," *Progress In Electromagnetics Research B*, Vol. 52, 383–403, 2013.

25. Agrawal, A., M. Misra, and A. Singh, "Oblique incidence and polarization insensitive multiband metamaterial absorber with quad paired concentric continuous ring resonators," *Progress In Electromagnetics Research M*, Vol. 60, 33–46, 2017.
26. Milligan, T. A., *Modern Antenna Design*, 2nd Edition, John Wiley & Sons Inc., IEEE Press, New Jersey, 2005.
27. Anguera, J., C. Punte, and C. Borja, "A procedure to design stacked microstrip patch antennas based on a simple network model," *Microwave and Optical Technology Letters*, Vol. 30, 149–151, 2001.
28. Jain, S. K. and S. Jain, "Performance analysis of coaxial fed stacked patch antennas," *Frequenz Journal of RF-Engineering and Telecommunication*, Vol. 68, Nos. 1–2, 7–18, 2014, doi: 10.1515/freq-2013-0073.
29. Smith, D. R., W. J. Padilla, D. C. Vier, S. C. Nemat-Nasser, and S. Schultz, "Composite medium with simultaneously negative permeability and permittivity," *Physics Review Letters*, Vol. 84, No. 10, 4184–4187, 1999.
30. Ha, J., K. Kwon, Y. Lee, and J. Choi, "Hybrid mode wideband patch antenna loaded with a planar metamaterial unit cell," *IEEE Transactions on Antennas and Propagation*, Vol. 60, No. 2, 1143–1147, 2012.